

Descriptellation: Deep Learned Constellation Descriptors for SLAM

Chunwei Xing^{*1}, Xinyu Sun^{*1}, Andrei Cramariuc¹, Samuel Gull¹, Jen Jen Chung¹, Cesar Cadena¹, Roland Siegwart¹, Florian Tschopp²

Abstract—Current global localization descriptors in Simultaneous Localization and Mapping (SLAM) often fail under vast viewpoint or appearance changes. Adding topological information of semantic objects into the descriptors ameliorates the problem. However, handcrafted topological descriptors extract limited information and they are not robust to environmental noise, drastic perspective changes, or object occlusion or misdetections. To solve this problem, we formulate a learning-based approach by constructing constellations from semantically meaningful objects and use Deep Graph Convolution Networks to map the constellation representation to a descriptor. We demonstrate the effectiveness of our Deep Learned Constellation Descriptor (Descriptellation) on the Paris-Rue-Lille and IQmulus datasets. Although Descriptellation is trained on randomly generated simulation datasets, it shows good generalization abilities on real-world datasets. Descriptellation outperforms the PointNet and handcrafted constellation descriptors for global localization, and shows robustness against different types of noise.

I. INTRODUCTION

A robot’s ability to estimate its own pose in the environment is crucial for many applications, such as autonomous driving, navigation, and trajectory tracking. SLAM [1] is proposed to address this problem. One crucial component is localization, i.e. finding its own location in a previously visited place. Currently, many methods perform localization using sparse appearance-based or object-based descriptors to build maps for robots.

Traditional appearance-based descriptors commonly used for local mapping achieve good performance in constructing locally consistent maps, as demonstrated by e.g. ORB-SLAM2 [2], SVO [3], and DSO [4]. However, due to visual odometry drift, systems based on visual keypoint descriptors, such as SIFT [5], SURF [6], BRIEF [7] and ORB [8], often fail to relocalize due to visual aliasing or changing visual appearances heavily impacted by changing perspectives, illumination, and object occlusion.

Object-based descriptors are proposed to solve the problem by using high-level representations, such as lines [9], cubes [10], and super quadrics [11]. Semantic information can also be attached to uniquely distinguish each object. Unlike appearance-based descriptors, instances can be robustly detected in the presence of changing perspectives, illumination, and object occlusion [11]. Some proposed

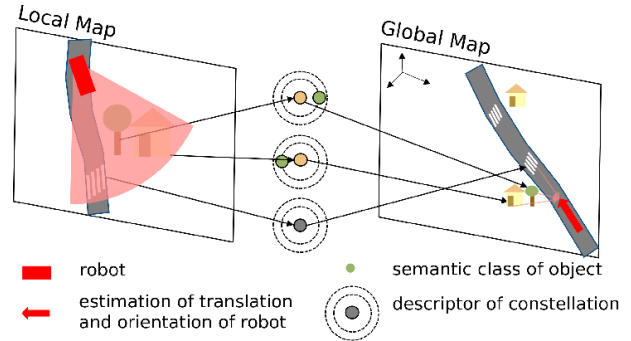


Fig. 1. Global localization based on semantic constellation descriptors. The global and local semantic object maps are considered as object constellations. For each object in the global and local map, we generate a graph by specifying an edge between every pair of neighboring nodes according to the Euclidean distance. The graph is used to extract robust descriptors using GCNs.

descriptors [9], [12] use the semantic label directly as a descriptor. However, this description method is often not distinct enough, especially when many objects have the same semantic label. It is time-consuming to pair target and query objects with such descriptors. In contrast, a semantic constellation with structural cues, consisting of an object and its neighbors, is likely to be unique for a given scene [13]. This allows us to interpret the structural and semantic information of a semantic object constellation as a descriptor for global localization.

GCNs show great potential in solving complex constellation classification problems [14], [15]. In this work, we introduce a learning-based semantic constellation descriptor combining both geometric and semantic information. An overview of our method is shown in Fig. 1. We develop a method to extract object constellations from object-centric maps and construct graphs from them. We incorporate GCNs for representation learning from object graphs with semantic information to obtain descriptors for global localization. Our work can be divided into three main contributions:

- A graph-level learned descriptor of fused geometric and semantic information extracted from semantic object constellation.
- A pipeline to train our deep-learned descriptor on simulation data and to apply it in a real-world application.
- Comparisons against existing baselines showing the feasibility and effectiveness of our model in terms of localization accuracy on real-world datasets.

^{*} Authors contribute to the work equally.

¹ Authors are with the Autonomous Systems Lab, ETH Zurich, Switzerland. {chxing, xinsun, crandrei, sgull, chungj, cesarc, rsiegwart}@ethz.ch.

² Author is with Arrival Ltd, United Kingdom, but the work was done while being a member of ¹, tschopp@arrival.com.

II. RELATED WORK

A. Descriptors

For the global localization problem in SLAM, many methods to generate a descriptor can be utilized, typically trading off between distinctiveness and robustness. In terms of whether high-level structural information is included, descriptors can be categorized as *individual* or *contextual*.

Individual descriptors generally extract local visual features of keypoints [16], [17] or geometric features of segments [18]–[20] and show high reliability in place recognition. Contextual descriptors such as VLAD [21], PointNetVLAD [22] and 3D Gestalt [23] aggregate features from neighborhoods and are more robust against noise. However, these descriptors are not rotation-invariant and perform poorly under large viewpoint changes.

Recently, contextual descriptors from semantic graphs [13], [24] have been used for place recognition, achieving rotation-invariant performance in several datasets. Semantic objects form the nodes of the graph as 3D points, which can be connected by edges based on e.g. proximity. Such graphs contain both geometric and semantic information, and thus can be used to extract fused features that are more robust to the aforementioned changes [24]. Random Walk descriptors as proposed by [13] and [25] achieve good performance on graph matching and localization. However, random walk descriptors implicitly utilize the topological information of the graph instead of the explicit geometric information, furthermore, performance varies with the walk steps and graph complexity.

B. Deep Learned Descriptors

Inspired by the great success of GCNs, [24], [26] used graph embeddings learned by the graph similarity network to match two graphs built from semantic maps. The graph networks concatenate the spatial-level and semantic-level features extracted by two separate edge convolution networks directly as the graph embedding. However, the geometric and semantic information could be combined as inputs and to extract fused features.

Graph representation learning methods can learn node-level and graph-level embeddings. Node-level embedding methods such as DeepWalk [27], node2vec [28], and Bag-of-Vectors [29] extract local graph structural information and project it onto lower dimensions. However, these methods lose the global structural information when extracting features. In Descriptellation, we propose a graph-level embedding as the descriptor of an object by aggregating node and edge features. GCNs extract structural information of neighboring nodes using spatial convolution operations.

In this paper, we use Deep Graph Convolution Network (Deep GCNs) [30] to extract node features and use the global attention layer [31] to aggregate all the features extracted by Deep GCNs into a fixed-length graph-level embedding which can be used as as the descriptor.

III. METHOD

In this section, we present our localization system based on Descriptellation. It leverages graph extraction from semantic

object-centric maps (III-A) and graph matching using graph descriptors (III-B) for global localization (III-C). Fig. 2 illustrates the architecture of our system, focusing on the graph representation and matching.

Our goal is to localize a robot by matching the locally built map (called *Query Local Submap (QLSM)*) with a previously recorded *global map*. In both maps, each node (object) is assigned to a learned descriptor by formulating its surrounding sub-constellation as a graph and extracting the graph’s features. Localization is achieved by matching descriptors of the QLSM to descriptors of the global map.

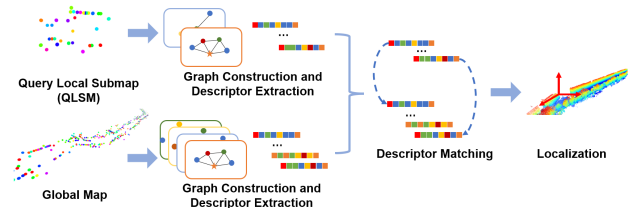


Fig. 2. Overview of the global localization system based on Descriptellation. For each object in the QLSM and the global map, a graph is built from the constellation of its neighboring objects, and its descriptor is extracted from the graph. By matching the descriptors in the QLSM with the database (descriptors extracted from each objects in the global map), candidate matching pairs can be found. By performing geometric verification on these matching pairs using RANSAC, a transformation matrix from the QLSM frame to the world frame can be obtained.

A. Object Constellation Extraction and Graph Generation

The global and local semantic object maps are considered as object constellations. For each object in the global and local map, we generate a graph by specifying an edge between every pair of neighboring objects (or nodes) according to the Euclidean distance within a predefined threshold, including the self-loop of the object itself. The threshold is defined by the average distance between two nodes in the global map.

B. Network Design for Representation Learning

As shown in Fig. 3, our network is adapted from Deep GCNs [30] consisting of the ResGCN backbone, a fusion block and a Multilayer Perceptron (MLP) prediction block. We modify the original network by adding an input embedding layer and an output global attention layer. The input of each node in the graph contains the 3D coordinates of its centroid (x, y, z) and an integer class label C . The integer labels merely represent an ordinal relationship among data. To solve this problem, we embed the semantic class into a 3-dimensional tensor (e_1, e_2, e_3) .

To extract features from node embeddings and edges, we use a 14-layer ResGCN as a backbone, and a Max-Relative convolution layer for convolution operations. The fusion block consists of a fully connected layer activated by a ReLU function and a max-pooling layer.

In order to aggregate the embeddings of all the nodes into a graph-level fixed-length embedding, an attention layer [31]

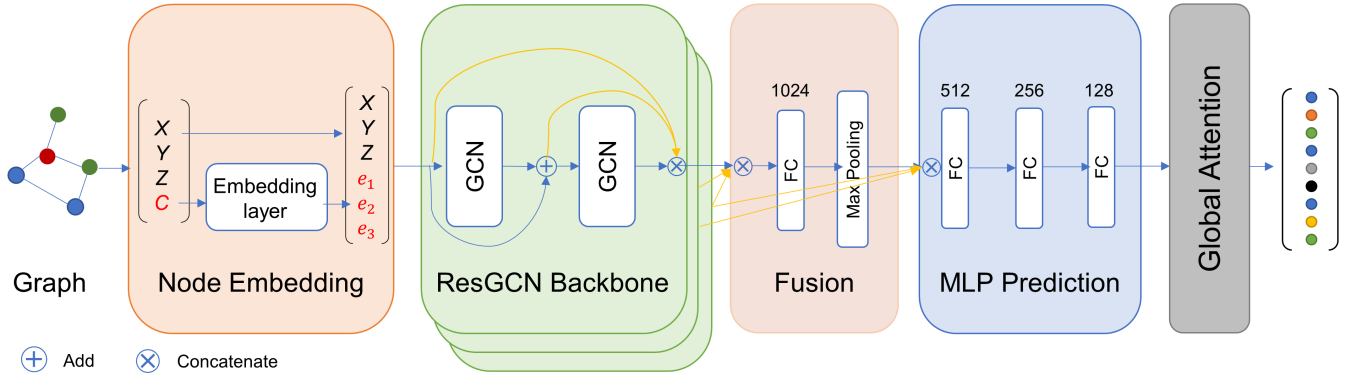


Fig. 3. Network architecture: Given a graph constructed according to Section III-A, the network integrates the spatial and semantic information of the edges and nodes to generate a graph descriptor using an extension of the Deep GCNs architecture [30]. The numbers above the fully connected (FC) blocks represent output sizes.

is used. It is a gated graph sequence neural network given by

$$\mathbf{r}_i = \sum_{n=1}^{N_i} \text{softmax}(h_{\text{gate}}(\mathbf{x}_n)) \odot h_{\theta}(\mathbf{x}_n), \quad (1)$$

where h_{gate} and h_{θ} are neural networks, \mathbf{x}_n denotes node features for node n , N_i is the number of nodes for batch index i , and \mathbf{r}_i denotes the batch-wise graph-level output. h_{θ} is the identity layer and \odot denotes element-wise multiplication. We utilize the batch triplet loss [32] to optimize the parameters at the training stage.

C. Global Localization

RANdom SAMple Consensus (RANSAC) [33] is frequently used for localization due to its robustness to outliers. In this section, we describe the matching process between the QLSM and the global map using RANSAC. For each object descriptor in the QLSM, its K closest descriptors in a given global map are found. RANSAC then performs feature-based registration by geometric verification given the predefined threshold t_{ransac} . Finally, the corresponding coordinates of these pairs are used to calculate the homogeneous transformation matrix T_{GL} from the local submap frame L to the global map frame G as

$$T_{GL} = \arg \min_{T_{GL}} \sum_{i=1}^k \left\| T_{GL} \begin{pmatrix} L\mathbf{p}^Li \\ 1 \end{pmatrix} - \begin{pmatrix} G\mathbf{p}^Gi \\ 1 \end{pmatrix} \right\|_2^2. \quad (2)$$

where \mathbf{p} is the i th 3D coordinates of the candidate pair in the QLSM frame L and global map frame G .

Addressing applications with observable gravity direction (e.g. ground vehicles or visual-inertial SLAM) we assume that the orientation of the local submap frame contains only non-zero yaw angle and zero pitch and roll angles. Furthermore, the translation along z is negligible. Thus we only optimize for (x, y, yaw) . Equation (2) can then be solved using an SVD solver, e.g. [34]. Nevertheless, the full 6 Degrees of Freedom (DoF) poses are still recoverable using the same method if the application requires it.

IV. TRAINING

A. Training Datasets & Implementation Details

1) *Data Generation*: The training dataset is created in a simple simulation environment by stochastically generating a series of object-centric maps with different objects. A map is populated by sub-constellations with various geometric shapes such as lines, circles, and multivariate normal distributions.

For each object, its constellation is first created as the anchor, consisting of randomly distributed sub-constellations and itself as a center node. The number of sub-constellations is $N_{\text{subcstl}} \sim \mathcal{U}\{5, 10\}$, where $\mathcal{U}\{a, b\}$ is a discrete uniform distribution in the integer set $\{a, a+1, \dots, b-1, b\}$. The number of nodes in each sub-constellation is $N_{\text{node}} \sim \mathcal{U}\{1, 20\}$. The coordinates of nodes in a sub-constellation are $x, y, z \sim \mathcal{U}(-1.0, 1.0)$, where $\mathcal{U}(a, b)$ is a continuous uniform distribution in the interval $[a, b]$. The number of objects in a constellation is $N_{\text{obj}} \sim \mathcal{U}\{10, 40\}$. The semantic class of a node is $C_{\text{node}} \sim \mathcal{U}\{0, 99\}$. By transforming the anchor constellation using 9 randomly sampled viewpoints, 9 positive samples are obtained. The graph is then constructed from the constellation using the method illustrated in Section III-A.

For the training and validation data, we generate 1000 anchor constellations and 9 positive constellations for each anchor using the strategy introduced above.

2) *Data Augmentation*: We simulate real-world data by adding ‘‘offline’’ noise to the datasets before training. Additionally, we add ‘‘online’’ noise to batch data when training the model to prevent overfitting at each epoch. The data augmentation methods are defined as follows:

- *Trans*: Translational noise is added to simulate the localization errors from upstream tasks, e.g. object mapping. This noise is added to each object in the constellation by

$$\tilde{\mathbf{p}}_{\text{object}} = \mathbf{p}_{\text{object}} + d(\mathbf{p}_{\text{origin}}, \mathbf{p}_{\text{object}}) \times e_{\text{trans}}, \quad (3)$$

where $\tilde{\mathbf{p}}$ defines a noisy position, $d(\mathbf{p}_{\text{origin}}, \mathbf{p}_{\text{object}})$ is the euclidean distance from the query object to the current object, $e_{\text{trans}} \sim \mathcal{U}(0, 0.05)$ for offline noise, and $e_{\text{trans}} \sim \mathcal{U}(0, 0.2)$ for online noise.

- *Orient*: To simulate perspective changes, orientational noise is added to the whole constellation, i.e., each object is rotated around the query’s z -axis by $r \sim \mathcal{U}(-180^\circ, 180^\circ)$ for both offline and online noise.
- *Dropout*: This noise is used to simulate the *false negative* ratio of an upstream task, e.g. object detection. We remove an object with a probability $p_{dropout} = 0.1$ for both offline and online *Dropout* noise.
- *FP*: This noise is implemented in the same context as *Dropout* noise, but instead representing the *false positive* ratio. We add a random object with a probability $p_{FP} = 0.1$ for both offline and online noise.
- *Misclass*: Misclassification noise represents the *error rate* in the context of a classification task. We change the class label of each object with a probability $p_{misclass} \times d(\mathbf{p}_{origin}, \mathbf{p}_{object})/d_{max}$ for both offline and online noise, where $d_{max} = \max\{d(\mathbf{p}_{origin}, \mathbf{p}_{object}^i)\}_{i=1}^{N_{obj}}$, and $p_{misclass} = 0.1$.
- *Crop*: We crop the constellation by removing objects along a ξ -axis if $\mathbf{p}_\xi > d_{max} \times (1 - p_{crop})$, where \mathbf{p}_ξ denotes the coordinates along $\xi \in \{x, y, z\}$ and $p_{crop} \sim \mathcal{U}(0, 0.3)$. The ξ -axis is chosen from $\{x, y, z\}$ with equal probability. We use this only for offline noise.
- *Scale*: The scale noise is applied to the whole constellation. The coordinates of each object are scaled according to the same factor $s \sim \mathcal{U}(0.85, 1.25)$. This is used only for online noise.

3) *Implementation*: The data is formulated in the Pytorch Geometric [35] format before being fed into the network, with the graph as the data and the graph index as the label. All the blocks of our model are trained from scratch at the same time. The full network is trained using the Adam optimizer [36] for 100 epochs, and the exponential decay rates β_1 and β_2 for the moment estimates are 0.9 and 0.999 respectively. The denominator term $\epsilon = 1 \times 10^{-8}$ for training stability, the initial learning rate is 1×10^{-3} , and the decay rate is 0.7. The training took approximately 3 hours on a NVIDIA GeForce GTX 1060 Ti GPU.

B. Training Results

We evaluate the training results using the *topK* ratio. In detail, for all constellation embeddings in the dataset, the K closest embeddings among all the other constellations are selected. The *topK* ratio is defined as the ratio of samples where at least one of the K selected embeddings has a matching label. The choice for K relates to the localization efficiency since the efficiency of RANSAC highly depends on the number of candidates. Tab. I shows the training results choosing $K = 5$.

We explore how to combine geometric information and semantic information by setting up experiments on different input types for our model with the same backbones and attention layers. The input types are as follows:

- (x, y, z) : This input contains only geometric information for comparison, i.e. coordinates of the object. The corresponding model called *Geo*.

- (x, y, z, C_{int}) : Besides geometric information, this input contains semantic information encoded by a scalar integer $C_{int} \in \{1, 2, \dots, N_{class}\}$. The corresponding model denoted as *Geo + Sem_Int*.
- (x, y, z, C_{onehot}) : This input encodes semantic information with one-hot encoding [37], i.e. $C_{onehot} \in \{0, 1\}^{N_{class} \times 1}$. The corresponding model is *Geo + Sem_Oh*.
- (x, y, z, C_{emd}) : This input encodes semantic information with learnable embeddings $C_{emd} \in \mathbb{R}^{N_{emd} \times 1}$. We use $N_{emd} = 3$ in our experiments. The corresponding model is *Geo + Sem_Emd*.

TABLE I
TRAINING RESULTS AT 100 TRAINING EPOCHS ON THE SIMULATED DATASETS.

Input	Evaluation Metrics					
	train loss	val loss	test loss	train top5	val top5	test top5
<i>Geo</i>	0.145	0.148	0.173	67.2%	81.7%	62.1%
<i>Geo + Sem_Int</i>	0.123	0.126	0.175	85.7%	94.4%	43.8%
<i>Geo + Sem_Oh</i>	0.0786	0.145	0.168	98.9%	90.0%	57.4%
<i>Geo + Sem_Emd</i>	0.0805	0.102	0.151	99.1%	98.1%	79.0%

We can conclude from Tab. I that the combination of geometric and semantic information is better than only using geometric information. Furthermore, a reasonable way to combine the geometric and semantic information is to first embed the semantic class into a multi-dimensional floating number and then concatenate them together with the geometric coordinates. We use this embedding-format model trained on the simulated training dataset to infer descriptors for global localization as shown in the following subsections.

V. EXPERIMENTS

A. Object-centric Maps Generation

To test the localization performance of our descriptor on real-world datasets, we used two outdoor point cloud datasets, Paris-Rue-Lille [38] and IQmulus [39]. These datasets contain fine-grained semantically and instance annotated point cloud data captured in a driving scenario.

We first generate object-centric maps from the point cloud datasets. The densely segmented global point cloud map is downsampled into voxels, each including 3D coordinates, instance ID, and semantic class ID. Voxels with dynamic semantic classes are removed. The centroid of an object is computed as the mean coordinates of voxels with the same instance ID. The global map is then composed of all the object centroids. Each *semantic object* is then represented by the 3D centroid coordinates, the instance ID and the semantic class label. To extract descriptors for such an object, we retrieve a local constellation for each semantic object in the global map. The local constellation is defined as a union of the object itself and its neighboring objects within a visual threshold.

B. Experiment Setup

When generating the test data, we first randomly sample query positions and orientations on the predefined sampling trajectory in the object-centric map. For each query position,

we first take the current visible static objects from the query position within a visual threshold to construct the *QLSM*, and we remove occluded objects [40]. We set the default visual threshold as 30 m in this paper. The coordinates of each object in the map are transformed into local coordinates with a random yaw angle to simulate an observation with unknown pose.

The process for object constellation extraction and graph generation follows Sec. III-A. By decreasing the visual threshold, we get fewer objects in the constellations which are harder to differentiate from each other. Since the datasets only contain a single trajectory, we perform localizing on the same data used to generate maps, i.e. *self-localization*. Nevertheless, we add observation noise to the constellations to simulate more realistic localization scenarios.

C. Global Localization Performance

We sample 500 query positions and orientations from each dataset and follow the pipelines demonstrated in Sec. III to compute the estimated positions and orientations. We evaluate the global localization performance by the success rate defined on the translation and orientation accuracy. In detail, the success rate η_{trans} is defined as the ratio of localized samples whose translation errors are less than $\tau_{trans} = 1$ m. The success rate η_{orient} is defined as the ratio of localized samples whose orientation errors are less than $\tau_{orient} = 5$ deg.

We propose 3 experiment cases to test the global localization performance of Descriptellation.

- *Self-localization*: Since the datasets contain only one trajectory, in this experiment we use exactly the same data in the *QLSM* as in the *global* map within the visual threshold. This scenario represents a perfect up-stream object mapping system.
- *Fewer Objects*: To simulate the realistic scenario where objects are deficient or they could only be reached in a limited range, we reduce the visible range from the centric object when building the *QLSM*.
- *Add Noise*: To represent a more realistic localization scenario, we introduce different kinds of noise, including *Trans*, *Dropout*, *Misclass*, and *Scale*. The noise is implemented in the same way as described in Sec. IV-A.2. For the *Trans* and *Scale* noise, we choose the error rate $e_{trans} \sim \mathcal{U}(0, 0.1)$ and scale ratio $s \sim \mathcal{U}(0.9, 1.1)$. For the *Dropout*, and *Misclass* noise, considering the the accuracy of state-of-the-art object detection and image classification models [41], we choose $p_{dropout} = 0.1$ and $p_{misclass} = 0.2$.

1) *Baselines*: We compared our model with 3 handcrafted descriptors and 1 learned descriptor as baselines. We term them *Onion Descriptor* (*Onion*), *Onion Histogram Descriptor* (*Onion Histogram*), *Random Walk Descriptor* (*Random Walk*), and *PointNet Descriptor* (*PointNet*).

The handcrafted descriptors are shown in Figure 4. For *Onion* and *Onion Histogram*, objects are split into n_s shells with equal distance between two neighboring shells d_s . *Onion* counts the number of objects in each shell as the descriptor. Similarly, *Onion Histogram* creates a histogram of objects'

semantic classes in the shells as the descriptor. For *Random Walk*, a number of n_w random walks of length l_w are sampled starting from the query object. The semantic class labels of the visited objects are stored in a descriptor matrix of shape $n_w \times l_w$. For *PointNet*, we adapt the original PointNet++ [42] by removing the soft-max layer at the end of the network and train on the same training data using the same triplet loss as our model.

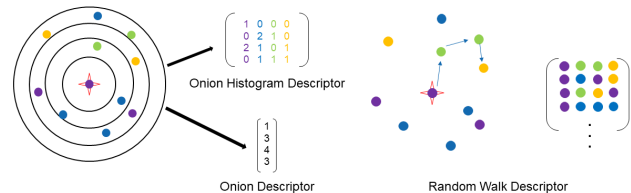


Fig. 4. Handcrafted baseline descriptors. The onion and onion histogram descriptor example shows the case when the number of shells $n_s = 4$ and number of classes $n_c = 4$. The random walk descriptor example shows the case when the walk length $l_w = 4$.

We tuned the parameters of the handcrafted baseline descriptors on simulation data. For *Onion* and *Onion Histogram*, we chose $n_s = 3$ and $d_s = 10$ m. For *Random Walk*, we chose the walk length $l_w = 4$ and the number of walks $n_w = 30$.

2) *Paris-Rue-Lille*: The Paris-Rue-Lille [38] is an urban point cloud dataset, containing 3 trajectories, Lille1, Lille2, and Paris. The dataset statistics are summarized in Table II. Dynamic and unknown objects are removed in pre-processing. We represent the objects using a 3D point located in the object's centroid [11] and reformulate the data format as $(x, y, z, instance\ id, class)$.

TABLE II
STATISTICS OF PARIS-RUE-LILLE DATASETS ($N_{obj, class}^b$ IS THE NUMBER OF OBJECTS AND CLASSES, RESPECTIVELY, $\{b, a\}$ IS BEFORE AND AFTER PREPROCESSING, RESPECTIVELY)

Trajectory	Length	N_{obj}^b	N_{class}^b	N_{obj}^a	N_{class}^a
Lille1	1150 m	1349	39	913	26
Lille2	340 m	501	29	331	20
Paris	450 m	629	41	306	23

Tab. III, IV, and V shows the localization performance of Descriptellation compared to the baselines on the Paris-Rue-Lille dataset. On Lille1, our model performs much better than the other descriptors in all cases. On Lille2, our model shows stronger robustness in *Fewer Objects* and *Add Noise* scenarios. On Paris, our model shows a general performance among the best descriptors. In contrast, *Onion* and *PointNet* perform badly in all cases.

On Lille1, from the results of the self-localization, both the *Random Walk* and the *Onion Histogram* have the descriptiveness to identify the constellations. Since these two descriptors only take vague spatial relations into account instead of specific distances among objects in the constellation, their descriptiveness can be weak when the number of spatial relations decreases, as is the case when the visual

TABLE III

GLOBAL LOCALIZATION SUCCESS RATES ON THE LILLE1 DATASET.

	Self-localization		Fewer Objects		Add Noise	
	η_{trans}	η_{orient}	η_{trans}	η_{orient}	η_{trans}	η_{orient}
<i>PointNet</i>	9.8%	20.4%	3.4%	11.2%	1.8%	6.8%
<i>Onion</i>	5.6%	11.2%	1.4%	8.0%	0.0%	5.6%
<i>Random Walk</i>	93.0%	96.0%	84.8%	90.0%	42.0%	62.8%
<i>Onion Histogram</i>	98.6%	98.8%	88.0%	91.6%	36.2%	53.0%
Ours	99.2%	99.2%	92.0%	96.6%	49.6%	69.4%

TABLE IV

GLOBAL LOCALIZATION SUCCESS RATES ON THE LILLE2 DATASET.

	Self-localization		Fewer Objects		Add Noise	
	η_{trans}	η_{orient}	η_{trans}	η_{orient}	η_{trans}	η_{orient}
<i>PointNet</i>	7.0%	18.6%	4.8%	11.4%	1.0%	7.2%
<i>Onion</i>	2.6%	9.8%	1.8%	5.8%	0.0%	4.2%
<i>Random Walk</i>	95.4%	96.2%	90.4%	91.8%	48.6%	65.8%
<i>Onion Histogram</i>	100.0%	99.6%	97.4%	97.8%	50.0%	61.0%
Ours	98.6%	98.8%	97.0%	97.8%	52.2%	67.8%

threshold is decreased in *Fewer objects*. However, our deep-learned descriptor learns directly from the graph with specific distances between each pair of objects. The descriptiveness is still powerful even if the constellations contain fewer semantic objects because the distances between objects is used to extract distinct features. As shown in Table III, when the visual threshold is decreased in the “Fewer Objects” case, our deep-learned descriptor shows better descriptiveness than other descriptors.

On *Lille1*, when adding noise, the performance of all the descriptors decreases. Among all the descriptors, our descriptor still performs the best on both the translation and orientation estimation accuracy thanks to being exposed to different kinds of noise during training.

In Fig. 5, we show the localization results on the *Lille1* dataset for the *Add Noise* case. As it illustrates, our descriptor outperforms all baselines in all resolutions.

3) *IQmulus Dataset*: The *IQmulus* database [39] is scanned from a dense urban environment and the statistics are shown in Tab. VI. In addition to removing dynamic objects, we remove the “bollard” class from the data because we found the distribution of these objects is very dense across the whole dataset. It decreases the performances of all descriptors significantly due to heavy self-similarity.

We also test 500 samples on the *IQmulus* dataset. The sampling process is the same as above. As shown in Table VII,

TABLE V

GLOBAL LOCALIZATION SUCCESS RATES ON THE PARIS DATASET.

	Self-localization		Fewer Objects		Add Noise	
	η_{trans}	η_{orient}	η_{trans}	η_{orient}	η_{trans}	η_{orient}
<i>PointNet</i>	3.2%	11.6%	6.2%	15.4%	9.6%	24.2%
<i>Onion</i>	13.2%	23.4%	4.6%	14.0%	2.2%	10.4%
<i>Random Walk</i>	92.2%	95.4%	66.6%	77.2%	45.0%	66.4%
<i>Onion Histogram</i>	95.6%	97.6%	77.8%	89.8%	41.4%	59.0%
Ours	91.4%	94.0%	67.2%	78.4%	42.0%	59.2%

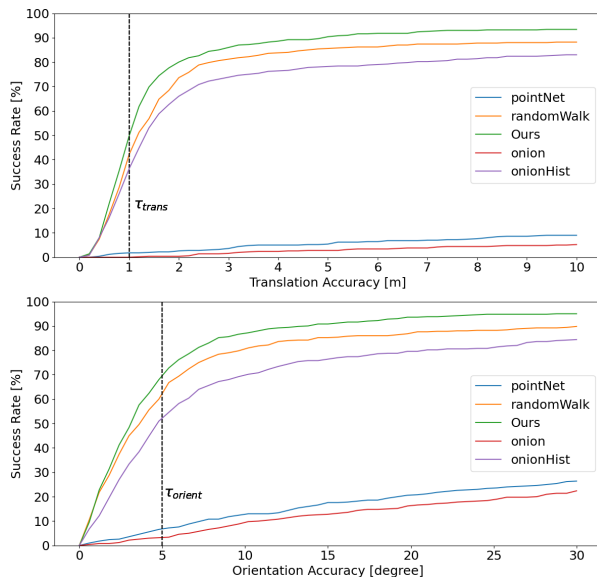


Fig. 5. Localization accuracy plot. The plot shows the performances on the *Lille1* dataset for the *Add Noise* case. Our descriptor shows advantages on both the translation and orientation accuracy.

TABLE VI
STATISTICS OF IQMULUS DATASETS

Trajectory	Length	N_{obj}^b	N_{class}^b	N_{obj}^a	N_{class}^a
Cassette	200 m	414	22	129	13

while not strictly outperforming all baselines, our model still shows the best overall performance and shows competitive results in all categories.

TABLE VII

GLOBAL LOCALIZATION SUCCESS RATES ON THE IQMULUS DATASET.

	Default Setting		Fewer Objects		Add Noise	
	η_{trans}	η_{orient}	η_{trans}	η_{orient}	η_{trans}	η_{orient}
<i>PointNet</i>	46.0%	52.4%	18.2%	23.0%	28.0%	38.6%
<i>Onion</i>	80.2%	75.0%	31.0%	32.6%	46.2%	42.6%
<i>Random Walk</i>	95.6%	95.6%	69.8%	79.6%	63.6%	66.4%
<i>Onion Histogram</i>	99.6%	96.6%	69.0%	67.0%	66.8%	53.8%
Ours	98.8%	93.4%	68.4%	79.2%	66.8%	61.4%

Compared to the *Lille1* dataset, the *IQmulus*, *Lille2*, and *Paris* dataset have much fewer objects and a shorter length, reducing the statistical strength of these experiments. Besides, for the *IQmulus* dataset, the object density reduces after removing the densely distributed “bollard” objects. The performance of *Random Walk*, *Onion Histogram* and our descriptor are much lower than on the *Lille1* datasets in the *Fewer objects* experiment, with greater similarity across the methods. This shows the influence of the object density and the distribution on the performance. The ambiguity may result from the self-similarity of the constellations or visual aliasing at different places. When the object distributions are similar to each other at different places, none of the tested descriptors are able to tell them apart and

our descriptor cannot extract more distinct descriptiveness from these constellations. Nevertheless, our descriptor still shows robustness against noise and performs generally well among the best descriptors.

VI. CONCLUSION

In this paper, we presented a graph convolution neural network architecture based on Deep GCNs and the attention mechanism to learn a set of object constellation descriptors for global localization in SLAM. We built up pipelines to extract deep-learned constellation descriptors from real-world point cloud data, and compared the global localization performance of our descriptor with handcrafted constellation descriptors and *PointNet*. The models used for the experiments are trained on simulation data for easy learning and data efficiency. Our deep-learned descriptors based on graph representation learning show good performance with a matching accuracy measured by the Top5 ratio close to 100% on simulation data, and a localization success rate of well over 90% in self-localization applications on real-world datasets

With Descriptellation, instead of relying on appearances to describe local features, we introduced a method to leverage higher-level semantic scene understanding and large-scale context, which enables localization in changing scenes. This is important since the number of detectable semantic classes is typically limited leading to self-similarity when only considering single objects in isolation.

As mentioned in Section V-C.3, our approach shares the sensitivity to anomaly object distributions with the other descriptors. However, we have the potential to resolve this problem thanks to the powerful learning ability of Deep GCNs. One possible solution is to enlarge the simulation database, e.g. to introduce more geometric shapes, when generating the training data. In addition, our training data can be optimized by simulating more realistic semantic object distributions or by fine-tuning on annotated real-world data. Our method could also be combined with other semantic object representations for better object matching results [11].

REFERENCES

- [1] C. Cadena, L. Carlone, H. Carrillo, Y. Latif, D. Scaramuzza, J. Neira, I. Reid, and J. Leonard, "Simultaneous localization and mapping: Present, future, and the robust-perception age," *IEEE Transactions on Robotics*, vol. 32, 06 2016.
- [2] R. Mur-Artal and J. Tardos, "ORB-SLAM2: an open-source SLAM system for monocular, stereo and RGB-D cameras," *IEEE Transactions on Robotics*, vol. PP, 10 2016.
- [3] C. Forster, M. Pizzoli, and D. Scaramuzza, "SVO: Fast semi-direct monocular visual odometry," 05 2014.
- [4] J. Engel, V. Koltun, and D. Cremers, "Direct sparse odometry," *IEEE Transactions on Pattern Analysis and Machine Intelligence*, vol. PP, 07 2016.
- [5] D. G. Lowe, "Distinctive image features from scale-invariant keypoints," *International journal of computer vision*, vol. 60, no. 2, pp. 91–110, 2004.
- [6] H. Bay, T. Tuytelaars, and L. Van Gool, "SURF: Speeded up robust features," vol. 110, 01 2006, pp. 404–417.
- [7] M. Calonder, V. Lepetit, C. Strecha, and P. Fua, "Brief: Binary robust independent elementary features," in *European conference on computer vision*, 2010, pp. 778–792.
- [8] E. Rublee, V. Rabaud, K. Konolige, and G. Bradski, "ORB: An efficient alternative to SIFT or SURF," in *2011 International Conference on Computer Vision*, 2011, pp. 2564–2571.
- [9] F. Taubner, F. Tschopp, T. Novkovic, R. Siegwart, and F. Furrer, "Lcd-line clustering and description for place recognition," in *2020 International Conference on 3D Vision (3DV)*, 2020, pp. 908–917.
- [10] S. Yang and S. Scherer, "Cubeslam: Monocular 3-d object slam," *IEEE Transactions on Robotics*, vol. 35, no. 4, pp. 925–938, 2019.
- [11] F. Tschopp, J. Nieto, R. Siegwart, and C. Cadena, "Superquadric object representation for optimization-based semantic SLAM," *arXiv preprint arXiv:2109.09627*, 2021.
- [12] N. Sünderhauf, S. Shirazi, F. Dayoub, B. Upcroft, and M. Milford, "On the performance of ConvNet features for place recognition," in *2015 IEEE/RSJ International Conference on Intelligent Robots and Systems (IROS)*, 2015, pp. 4297–4304.
- [13] A. Gawel, C. Del Don, R. Siegwart, J. Nieto, and C. Cadena, "X-view: Graph-based semantic multi-view localization," *IEEE Robotics and Automation Letters*, vol. 3, no. 3, pp. 1687–1694, 2018.
- [14] T. N. Kipf and M. Welling, "Semi-supervised classification with graph convolutional networks," in *5th International Conference on Learning Representations, ICLR 2017, Toulon, France, April 24-26, 2017, Conference Track Proceedings*, 2017.
- [15] Y. Wang, Y. Sun, Z. Liu, S. E. Sarma, M. M. Bronstein, and J. M. Solomon, "Dynamic graph cnn for learning on point clouds," *Acm Transactions On Graphics (tog)*, vol. 38, no. 5, pp. 1–12, 2019.
- [16] S. Salti, F. Tombari, and L. D. Stefano, "SHOT: Unique signatures of histograms for surface and texture description," *Comput. Vis. Image Underst.*, vol. 125, pp. 251–264, 2014.
- [17] J. Guo, P. V. Borges, C. Park, and A. Gawel, "Local descriptor for robust place recognition using lidar intensity," *IEEE Robotics and Automation Letters*, vol. 4, no. 2, pp. 1470–1477, 2019.
- [18] R. Dube, D. Dugas, E. Stumm, J. Nieto, R. Siegwart, and C. Cadena, "SegMatch: Segment based place recognition in 3D point clouds," 05 2017, pp. 5266–5272.
- [19] R. Dubé, A. Cramariuc, D. Dugas, J. Nieto, R. Siegwart, and C. Cadena, "SegMap: 3d segment mapping using data-driven descriptors," *arXiv preprint arXiv:1804.09557*, 2018.
- [20] A. Cramariuc, F. Tschopp, N. Alatur, S. Benz, T. Falck, M. Brühlmeier, B. Hahn, J. Nieto, and R. Siegwart, "SemSegMap – 3d segment-based semantic localization," in *2021 IEEE/RSJ International Conference on Intelligent Robots and Systems (IROS)*, 2021, pp. 1183–1190.
- [21] R. Arandjelovic and A. Zisserman, "All about vlad," in *Proceedings of the IEEE conference on Computer Vision and Pattern Recognition*, 2013, pp. 1578–1585.
- [22] M. A. Uy and G. H. Lee, "Pointnetvlad: Deep point cloud based retrieval for large-scale place recognition," in *Proceedings of the IEEE Conference on Computer Vision and Pattern Recognition*, 2018, pp. 4470–4479.
- [23] M. Bosse and R. Zlot, "Place recognition using keypoint voting in large 3D lidar datasets," in *2013 IEEE International Conference on Robotics and Automation*, 2013, pp. 2677–2684.
- [24] X. Kong, X. Yang, G. Zhai, X. Zhao, X. Zeng, M. Wang, Y. Liu, W. Li, and F. Wen, "Semantic graph based place recognition for 3d point clouds," 10 2020, pp. 8216–8223.
- [25] Y. Liu, Y. Petillot, D. Lane, and S. Wang, "Global localization with object-level semantics and topology," in *2019 International Conference on Robotics and Automation (ICRA)*. IEEE, 2019, pp. 4909–4915.
- [26] Z. Zhang, P. Cui, and W. Zhu, "Deep learning on graphs: A survey," *IEEE Transactions on Knowledge and Data Engineering*, vol. PP, pp. 1–1, 03 2020.
- [27] B. Perozzi, R. Al-Rfou, and S. Skiena, "DeepWalk: Online learning of social representations," *Proceedings of the ACM SIGKDD International Conference on Knowledge Discovery and Data Mining*, 03 2014.
- [28] A. Grover and J. Leskovec, "node2vec: Scalable feature learning for networks," vol. 2016, 07 2016, pp. 855–864.
- [29] G. Nikolentzos, P. Meladianos, and M. Vazirgiannis, "Matching node embeddings for graph similarity," in *Proceedings of the Thirty-First AAAI Conference on Artificial Intelligence*, ser. AAAI'17, 2017, pp. 2429–2435.
- [30] G. Li, M. Müller, A. Thabet, and B. Ghanem, "DeepGCNs: Can GCNs Go as Deep as CNNs?" in *The IEEE International Conference on Computer Vision (ICCV)*, 2019.
- [31] Y. Li, D. Tarlow, M. Brockschmidt, and R. Zemel, "Gated graph sequence neural networks," *arXiv preprint arXiv:1511.05493*, 2015.
- [32] A. Hermans*, L. Beyer*, and B. Leibe, "In Defense of the Triplet Loss for Person Re-Identification," *arXiv preprint arXiv:1703.07737*, 2017.

- [33] M. A. Fischler and R. C. Bolles, "Random sample consensus: a paradigm for model fitting with applications to image analysis and automated cartography," *Communications of the ACM*, vol. 24, no. 6, pp. 381–395, 1981.
- [34] O. Sorkine, "Least-squares rigid motion using svd," *Technical notes*, vol. 120, no. 3, p. 52, 2009.
- [35] M. Fey and J. E. Lenssen, "Fast graph representation learning with PyTorch Geometric," in *ICLR Workshop on Representation Learning on Graphs and Manifolds*, 2019.
- [36] D. Kingma and J. Ba, "Adam: A method for stochastic optimization," *International Conference on Learning Representations*, 12 2014.
- [37] H. Alkharusi, "Categorical variables in regression analysis: A comparison of dummy and effect coding," *International Journal of Education*, vol. 4, no. 2, p. 202, 2012.
- [38] X. Roynard, J.-E. Deschaud, and F. Goulette, "Paris-Lille-3D: A large and high-quality ground-truth urban point cloud dataset for automatic segmentation and classification," *The International Journal of Robotics Research*, vol. 37, no. 6, pp. 545–557, 2018.
- [39] B. Vallet, M. Brédif, A. Serna, B. Marcotegui, and N. Paparoditis, "Ter-Mobilita/iQmulus urban point cloud analysis benchmark," *Computers and Graphics*, vol. 49, pp. 126–133, 2015.
- [40] S. Katz, A. Tal, and R. Basri, "Direct visibility of point sets," *ACM Trans. Graph.*, vol. 26, no. 3, p. 24–es, Jul. 2007.
- [41] S. Vora, A. H. Lang, B. Helou, and O. Beijbom, "Pointpainting: Sequential fusion for 3d object detection," in *Proceedings of the IEEE/CVF conference on computer vision and pattern recognition*, 2020, pp. 4604–4612.
- [42] C. R. Qi, H. Su, K. Mo, and L. J. Guibas, "Pointnet: Deep learning on point sets for 3d classification and segmentation," in *Proceedings of the IEEE conference on computer vision and pattern recognition*, 2017, pp. 652–660.